J|A|C|S
ARTICLES
Published on Web 02/06/2007

Conductivity in Alkylamine/Gold and Alkanethiol/Gold Molecular Junctions Measured in Molecule/Nanoparticle/Molecule Bridges and Conducting Probe Structures

Changwoong Chu, Jeong-Seok Na, and Gregory N. Parsons*

Contribution from the Department of Chemical & Biomolecular Engineering, North Carolina State University, Raleigh, North Carolina 27695

Received July 12, 2006; E-mail: parsons@ncsu.edu

Abstract: Charge transport through alkane monolayers on gold is measured as a function of molecule length in a controlled ambient using a metal/molecule/nanoparticle bridge structure and compared for both thiol and amine molecular end groups. The current through molecules with an amine/gold junction is observed to be more than a factor of 10 larger than that measured in similar molecules with thiol/gold linkages. Conducting probe atomic force microscopy is also used to characterize the same monolayer systems, and the results are quantitatively consistent with those found in the nanoparticle bridge geometry. Scaling of the current with contact area is used to estimate that ~100 molecules are probed in the nanoparticle bridge geometry. For both molecular end groups, the room-temperature conductivity at low bias as a function of molecule length shows a reasonable fit to models of coherent nonresonant charge tunneling. The different conductivity is ascribed to differences in charge transfer and wave function mixing at the metal/molecule contact, including possible effects of amine group oxidation and molecular conformation. For the amine/Au contact, the nitrogen lone pair interaction with the gold results in a hybrid wave function directed along the molecule bond axis, whereas the thiol/Au contact leads to a more localized wave function.

1. Introduction

The nature of the coupling between organic molecules and solid inorganic materials is critically important for the function and performance of many advanced molecular and organic electronic devices. In addition, charge transport in molecules is important in many chemical and biochemical systems, and an improved understanding of electron-transport processes could open new possibilities for engineered molecular devices. For the case of metal/molecule contacts, a particularly important question is how the charge transport through the junction is controlled by the mixing between discrete orbitals in a molecule and the continuum states in a metal.[1−5] The relatively large density of states in the metal will act to broaden and shift the molecular states from their energies in a vacuum, so that the metal/molecule/metal structure should be considered to act as a single molecular junction unit.[2,6−8] Even so, the conductance through the junction will be affected by both the overlap of the orbitals in the contact region and the spatial arrangement and symmetry of the molecular orbitals in the bridge. Many studies have focused on differentiating the role of the contacts from that of the molecular structure on charge transport mechanisms. Often, the metal, contacting end group, and/or molecule structure are individually modified, and the effect of the change on the overall junction is subsequently analyzed.[1,6,9−20] In many cases, it is found that relatively small changes in the metal/molecule contact can have a pronounced effect on charge flow, similar to the effect of a relatively large change in the molecular bridge.[1,12,16] This observation points to the importance of the molecule/metal interface in understanding charge transfer in metal/molecule/metal junctions. In this article, conduction through saturated chain self-assembled monolayers is measured

(1) Selzer, Y.; Salomon, A.; Cahen, D. *J. Phys. Chem. B* **2002**, *106*, 10432−10439.
(2) Nitzan, A.; Ratner, M. A. *Science* **2003**, *300*, 1384−1389.
(3) Datta, S. *Nanotechnology* **2004**, *15*, S433−S451.
(4) Selzer, Y.; Cai, L.; Cabassi, M. A.; Yao, Y.; Tour, J. M.; Mayer, T. S.; Allara, D. L. *Nano Lett.* **2005**, *5*, 61−65.
(5) Troisi, A.; Ratner, M. *Small* **2006**, *2*, 172−181.
(6) Cui, X. D.; Primak, A.; Zarate, X.; Tomfohr, J.; Sankey, O. F.; Moore, A. L.; Moore, T. A.; Gust, D.; Nagahara, L. A.; Lindsay, S. M. *J. Phys. Chem. B* **2002**, *106*, 8609−8614.
(7) James, D. K.; Tour, J. M. *Chem. Mater.* **2004**, *16*, 4423−4435.
(8) McCreery, R. *Chem. Mater.* **2004**, *16*, 4477−4496.
(9) Wold, D. J.; Frisbie, C. D. *J. Am. Chem. Soc.* **2001**, *123*, 5549−5556.
(10) Fan, F.-R. F.; Yang, J.; Cai, L.; Price, D. W., Jr.; Dirk, S. M.; Kosynkin, D. V.; Yao, Y.; Rawlett, A. M.; Tour, J. M.; Bard, A. J. *J. Am. Chem. Soc.* **2002**, *124*, 5550−5560.
(11) Kushmerick, J. G.; Holt, D. B.; Pollack, S. K.; Ratner, M. A.; Yang, J. C.; Schull, T. L.; Naciri, J.; Moore, M. H.; Shashidhar, R. *J. Am. Chem. Soc.* **2002**, *124*, 10654−10655.
(12) Beebe, J. M.; Engelkes, V. B.; Miller, L. L.; Frisbie, C. D. *J. Am. Chem. Soc.* **2002**, *124*, 11268−11269.
(13) Anariba, F.; McCreery, R. L. *J. Phys. Chem. B* **2002**, *106*, 10355−10362.
(14) Chen, J.; Wang, W.; Klemic, J.; Reed, M. A.; Axelrod, B. W.; Kaschak, D. M.; Rawlett, A. M.; Price, D. W.; Dirk, S. M.; Tour, J. M.; Grubisha, D. S.; Bennett, D. W. *Ann. N.Y. Acad. Sci.* **2002**, *960*, 69−99.
(15) Metzger, R. M. *Chem. Rev* **2003**, *103*, 3803−3834.
(16) Engelkes, V. B.; Beebe, J. M.; Frisbie, C. D. *J. Am. Chem. Soc.* **2004**, *126*, 14287−14296.
(17) Blum, A. S.; Kushmerick, J. G.; Pollack, S. K.; Yang, J. C.; Moore, M.; Naciri, J.; Shashidhar, R.; Ratna, B. R. *J. Phys. Chem. B* **2004**, *108*, 18124−18128.
(18) Haick, H.; Ghabboun, J.; Cahen, D. *Appl. Phys. Lett.* **2005**, *86*, 042113.
(19) Long, D. P.; Patterson, C. H.; Moore, M. H.; Seferos, D. S.; Bazan, G. C.; Kushmerick, J. G. *Appl. Phys. Lett.* **2005**, *86*, 1610.
(20) Dadosh, T.; Gordin, Y.; Krahne, R.; Khivrich, I.; Mahalu, D.; Frydman, V.; Sperling, J.; Yacoby, A.; Bar-Joseph, I. *Nature* **2005**, *436*, 677−680.

and directly compared for the widely studied Au/thiol contact and the less studied Au/amine interface.

Many techniques have been used to characterize molecule/metal junctions, including scanning tunneling microscopy (STM),[21−23] mechanical break junctions,[24,25] conducting probe atomic force microscopy (CPAFM),[9,16,26−30] crossed gold wires,[11,17,31] liquid mercury drops,[32,33] and several others. Several recent reviews have discussed and contrasted these methods.[2,7,8,34,35] A significant problem in many fabrication approaches is that metal deposition may damage molecular layers, and techniques for indirect metal evaporation have been developed to address this issue.[18,36] Another approach to control molecular contacts is to use metal particles bridged between organic monolayers formed on metallic electrodes.[19,20,37] In this technique, a symmetric metal/molecule/nanoparticle/molecule/metal bridge is formed, and the current through the two molecular layers is measured in series and characterized. In addition to minimizing potential damage, the symmetric structure eliminates the force loading dependence on conduction which is observed in conducting probe studies.[9,29,30] Furthermore, the nanoparticle bridge approach enables characterization in a common probe station without the need for the scanning probe electronics, and it could be used to connect together multiple molecular junctions. Previous studies using the nanoparticle bridge approach focused primarily on conductance through conjugated molecules with thiol terminal groups linked to gold. Amlani et al.[37] demonstrated the particle bridge concept by measuring conductance through a monolayer of (1-nitro-2,5-diphenylethynyl-4′-thioacetyl)benzene. Long et al.[19] demonstrated magnetic nanoparticle assembly by comparing conductance through undecanethiol, oligo(phenylene ethynylene)-dithiol, and oligo(phenylene vinylene)dithiol. Dadosh et al.[20] extended this approach to include analysis of three different conjugated dithiol molecules assembled between nanoparticles, where the particle bridge then enabled analysis of single molecules.

In this article, the molecule/nanoparticle bridge technique is utilized to analyze room-temperature conduction in alkane molecule systems as a function of molecule length and surface contact group. At low bias, the thickness dependence of the room-temperature current−voltage curves are consistent with coherent nonresonant charge tunneling through the alkane layers.[9,25,29] We have fit the data to a common model for nonresonant tunneling,[38] and values for the effective tunneling barrier heights and tunneling decay constant, β, are estimated. Trends in charge conductance are examined for alkane molecules contacted to gold electrodes with methyl, thiol, and amine end groups. Performing measurements in a nanoparticle bridge geometry and in a conducting force probe structure, the current through alkanes with an amine/gold contact is found to be consistently larger than for the same molecule with a thiol/gold contact. Possible mechanisms that could account for the larger current flow through the amine-terminated structure versus the thiol bond are presented.

2. Experimental Approach

Preparation of Electrical Test-Beds. Metallic "nanogap" electrodes were fabricated using micrometer-scale patterned metal films and oblique angle metal evaporation.[39] The electrodes were formed using the sharp edge of a lithographically patterned metal layer deposited on thermally grown SiO_2-coated silicon(100) wafers. Gold (90 nm in thickness) on a titanium (10 nm) layer was evaporated at approximately 1 Å/s in an electron-beam evaporator at $\sim 5 \times 10^{-6}$ Torr. Figure 1a shows schematically the patterned photoresist with a large ($\sim 20\ \mu$m) separation. The contact pads are $100 \times 100\ \mu m^2$. The patterned metals were etched by chemicals such as aqua regia for gold ($HCl:HNO_3:H_2O = 1:1:1$) and titanium etchant for titanium (Transene Co., Inc., Danvers MA). After the photoresist was stripped (Figure 1b), the second metal was evaporated at an oblique angle, as shown in Figure 1c,g. Since the oblique metallization (metal-2) covers the entire area except the region shadowed by metal-1, a second lithography step was needed to complete the fabrication (Figure 1d,e). The nanoscale shadowed region without metal deposition remained between probing pads, resulting in a nanoscale gap, as illustrated in Figure 1e. Figure 1h shows an AFM image of the final shape of the nanoscale gap between two Au/Ti electrodes, and the AFM data were used to measure the resulting gap dimension. The current−voltage measurement of the nanoscale gap shows a negligible current level of $\sim 10^{-14}$ A, confirming that the resulting nanoscale gap is an open circuit.

SAM Preparation and Nanoparticle Assembly. For the electronic conduction study, self-assembled molecular monolayers of a range of molecules, including thiol- and amine-terminated alkanes, were formed on the Au/Ti nanoelectrodes. Molecules included 1-hexanethiol (C6SH), 1-decanethiol (C10SH), 1-dodecanethiol (C12SH), 1-aminohexane (C6NH), 1-aminodecane (C10NH), 1-aminododecane (C12NH), and 1-aminooctadecane (C18NH). For the formation of a complete self-assembled monolayer (SAM), the starting nanogap gold electrodes were treated with ultraviolet ozone cleaner and then rinsed with high-purity ethanol. After they were dried with flowing nitrogen,

(21) Joachim, C.; Gimzewski, J. K.; Schlittler, R. R.; Chavy, C. *Phys. Rev. Lett.* **1995**, *74*, 2102−2105.
(22) Bumm, L. A.; Arnold, J. J.; Cygan, M. T.; Dunbar, T. D.; Burgin, T. P.; Jones, L.; Allara, D. L.; Tour, J. M.; Weiss, P. S. *Science* **1996**, *271*, 1705−1707.
(23) Cui, X. D.; Primak, A.; Zarate, X.; Tomfohr, J.; Sankey, O. F.; Moore, A. L.; Moore, T. A.; Gust, D.; Harris, G.; Lindsay, S. M. *Science* **2001**, *294*, 571−574.
(24) Reed, M. A.; Zhou, C.; Muller, C. J.; Burgin, T. P.; Tour, J. M. *Science* **1997**, *278*, 252−254.
(25) Kergueris, C.; Bourgoin, J. P.; Palacin, S.; Esteve, D.; Urbina, C.; Magoga, M.; Joachim, C. *Phys. Rev. B* **1999**, *59*, 12505−12513.
(26) Kelley, T. W.; Granstrom, E. L.; Frisbie, C. D. *Adv. Mater.* **1999**, *11*, 261−264.
(27) Wold, D. J.; Frisbie, C. D. *J. Am. Chem. Soc.* **2000**, *122*, 2970−2971.
(28) Wold, D. J.; Haag, R.; Rampi, M. A.; Frisbie, C. D. *J. Phys. Chem. B* **2002**, *106*, 2813−2816.
(29) Cui, X. D.; Zarate, X.; Tomfohr, J.; Sankey, O. F.; Primak, A.; Moore, A. L.; Moore, T. A.; Gust, D.; Harris, G.; Lindsay, S. M. *Nanotechnology* **2002**, *13*, 5−14.
(30) Ishida, T.; Mizutani, W.; Liang, T.-T.; Azehara, H.; Miyake, K.; Sasaki, S.; Tokumoto, H. Conductive Probe AFM Measurements of Conjugated Molecular Wires. In *Molecular Electronics III*; Reimers, J. R., Picconatto, C. A., Ellenbogen, J. C., Shashidhar, R., Eds.; Annals of the New York Academy of Sciences 1006; New York Academy of Sciences: New York, 2003.
(31) Kushmerick, J. G.; Naciri, J.; Yang, J. C.; Shashidhar, R. *Nano Lett.* **2003**, *3*, 897−900.
(32) Rampi, M. A.; Schueller, O. J. A.; Whitesides, G. M. *Appl. Phys. Lett.* **1998**, *72*, 1781−1783.
(33) Slowinski, K.; Fong, H. K. Y.; Majda, M. *J. Am. Chem. Soc.* **1999**, *121*, 7257−7261.
(34) McCreery, R. L. *Anal. Chem. A-Pages* **2006**, *78*, 3490−3497.
(35) Selzer, Y.; Allara, D. L. *Annu. Rev. Phys. Chem.* **2006**, *57*, 593−623.
(36) Metzger, R.; Xu, T.; Peterson, I. *J. Phys. Chem. B* **2001**, *105*, 7280.
(37) Amlani, I.; Rawlett, A. M.; Nagahara, L. A.; Tsui, R. K. *Appl. Phys. Lett.* **2002**, *80*, 2761−2763.
(38) Simmons, J. G. *J. Appl. Phys.* **1963**, *34*, 1793.
(39) Dolan, G. J. *Appl. Phys. Lett.* **1977**, *31*, 337−339.

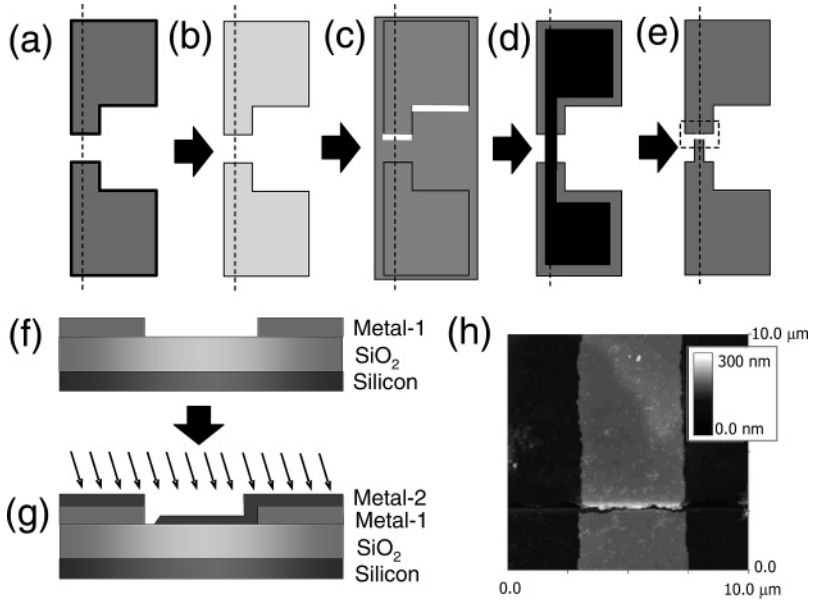

Figure 1. Fabrication procedure for nanoscale gap: (a)−(e) plane views and (f),(g) cross-sectional views of patterns of the proposed processes. The schematics in panels a−g are not scaled, and the thickness of each layer and space widths are exaggerated for simple explanation. The arrows in panel g are the imagined trajectory of evaporated metal molecules. The broken lines in panels a−e indicate the cross-section lines for panels f and g. Panel a shows the patterns of defined photoresist on the first metal layer as a plane view. Panel b shows the patterned metal after etching with photoresist mask. Its cross-sectional shape is shown in panel f. Panel c shows the second metal layer after deposition with an oblique angle, which is illustrated in panel g. White lines in panel c indicate the shadowed region during second metallization, while all the other areas are covered with the metal. Panel d shows the photoresist pattern on second metal, and panel e shows the final shape of the metal pad whose gap is ∼50 nm. Panel h shows the AFM image of the nanoscale gap area in panel e, which proves the disconnection of the two electrodes.

the clean samples were preserved in the filtered argon-purged vials to minimize contamination from any organics and oxygen. The SAM of interest was dissolved in organic solvent (1 mM in ethanol for alkanethiols and tetrahydrofuran or hexane for alkylamines), the solution was injected into the argon-purged vial by disposable syringe with a 200 μm filter, and the sample was left for more than 24 h to form a complete monolayer.[40] Removal of molecules not bonded to the surface was achieved by rinsing them with a copious amount of ethanol and drying with flowing nitrogen. Ellipsometry results measured on planar surfaces indicate the thicknesses of the alkanethiol SAMs are 6.7 (C6SH), 11.0 (C10SH), and 13.0 Å (C12SH).

Self-assembly of alkylamine molecules has been investigated by several groups on planar gold surfaces[41] and on gold nanoparticles.[42−44] In contrast to the alkanethiols, amine-terminated *n*-alkanes spontaneously adsorb on the Au surfaces from nonpolar solvents, and they are believed to be stable for periods of at least several hours.[41] However, in polar solvents, the Au vs N interaction energy is not strong enough to lead to highly stable monolayers.[41,45] For the studies reported here, alkylamine SAMs were formed on gold from hexane solution, where the film was left to form for 48 h. The thicknesses of alkylamine SAMs were measured using ellipsometry to be 6.7 (C6NH), 12.0 (C10NH), 13.0 (C12NH), and 19.7 Å (C18NH), consistent with the expected monolayer thicknesses.

After SAM formation on the nanogap electrodes, citrate-capped Au nanoparticles (Ted Pella, Inc., Redding, CA) of ∼80 nm diameter (i.e., larger than the 50 nm electrode gap spacing) were deposited into the nanogap region to complete the electrical test circuit, followed by immediate transfer into the vacuum (<1 mTorr) probe station. When the amine molecules were incubated with the Au/Ti electrodes prior to exposure to the Au nanoparticles, the molecules were expected to arrange with the amine groups bound on the Au/Ti electrodes and the methyl tails adjacent to the Au nanoparticle. This arrangement is similar to that expected for the case of the alkanethiols. This approach thereby forms two molecular junctions in series, consisting of (i) a set of gold/thiol bonds between the gold electrode and the set of molecules in the left-side junction, (ii) a set of methyl/gold physical bonds between the nanoparticle and the molecules in the left-side junction, (iii) another set of methyl/gold physical bonds in the right-side junction, and (iv) another set of gold/thiol bonds between the gold electrode and the molecules in the right-side junction. This work addresses the role of the bond between the gold electrode and the monolayer by studying the conductance change that occurs when the gold/thiol bonds are replaced with gold/amine bonds in the molecular junctions. To this end, several different methods were evaluated to assemble the 80 nm nanoparticles along the gap. Previous results showed that an electrophoretic force with direct current[46] and a dielectrophoretic force with alternative current[47,48] can be used to pull nanoparticles into a nanoscale gap. A more direct method, using nanoparticle solution drops in the gap area, has been

(40) Ohgi, T.; Sheng, H.-Y.; Nejoh, H. *Appl. Surf. Sci.* **1998**, *130−132*, 919−924.
(41) Xu, C. J.; Sun, L.; Kepley, L. J.; Crooks, R. M.; Ricco, A. J. *Anal. Chem.* **1993**, *65*, 2102−2107.
(42) Brown, L. O.; Hutchison, J. E. *J. Am. Chem. Soc.* **1999**, *121*, 882−883.
(43) Chen, X. Y.; Li, J. R.; Jiang, L. *Nanotechnology* **2000**, *11*, 108−111.
(44) Kumar, A.; Mandal, S.; Selvakannan, P. R.; Pasricha, R.; Mandale, A. B.; Sastry, M. *Langmuir* **2003**, *19*, 6277−6282.
(45) Ruan, C. M.; Bayer, T.; Meth, S.; Sukenik, C. N. *Thin Solid Films* **2002**, *419*, 95−104.
(46) Bezryadin, A.; Dekker, C.; Schmid, G. *Appl. Phys. Lett.* **1997**, *71*, 1273−1275.
(47) Lumsdon, S. O.; Kaler, E. W.; Williams, J. P.; Velev, O. D. *Appl. Phys. Lett.* **2003**, *82*, 949−951.
(48) Xia, Y. N.; Yin, Y. D.; Lu, Y.; McLellan, J. *Adv. Funct. Mater.* **2003**, *13*, 907−918.

developed and used here primarily. In this method, the nanoparticle solution drop forms a meniscus near the probing needle. While most particles remain elsewhere on the surface outside the region of interest and do not affect the measurement, a small number of particles enter into the gap due to the dragging force of the withdrawing water meniscus. We find that connections can be made at about the same rate with these methods. The citrate stabilizing molecules on the gold nanoparticles are not expected to significantly affect the resistance measurement. While detailed effects of the citrate molecules cannot be ruled out, we presume that the absorption of nanoparticles on methyl-terminated monolayers results in similar interface bond structure in all such junctions studied. For the case of nanoparticle assembly onto molecules with binding groups in both ends, after nanoparticle adsorption, the unbound nanoparticles were rinsed with deionized water and then dried with a gentle flow of nitrogen. This sample preparation method was found to be reasonably reproducible and reliable, without requiring a burdensome set of trials for quantitative results, and it enabled measurement with minimal exposure to ambient.

Figure 2a shows AFM images of ~80 nm nanoparticles forming a bridge between the two disconnected monolayers across the gap distance of ~50 nm. The nanoparticles bridging the nanogap are shown in the circled areas. Figure 2d shows a scaled sketch of the cross section of the structure with a nanoparticle in place, based on the AFM image scans. Figure 2b shows the AFM image of an example nanogap structure after nanoparticle assembly, where no particle connections are made across the gap region. In both panels a and b of Figure 2, nanoparticles are also observed dispersed on the electrodes away from the contact gap region. Conduction is observed for the electrodes in Figure 2a, but not for the electrodes in Figure 2b, confirming that the nanoparticle bridge in Figure 2a completes the electrical circuit.

3. Current versus Voltage Results

Current through Metal/Nanoparticle/Metal Structures. The current−voltage ($I-V$) behavior of three different nanoparticle-bridged gold nanogaps, measured in a vacuum (<1 mTorr) with no molecule layer intentionally adsorbed on the gold electrodes, is shown in Figure 2c. The behavior is shown to be linear, and junction resistances of 55.2, 44.2, and 32.9 Ω are measured when the nanoelectrode gap is observed by AFM to contain, respectively, two, three, and four nanoparticle bridges in parallel. The resistance values are consistent with the nanoparticle bridges acting as parallel conductance paths, with the resistance of one particle ranging from 110 to 132 Ω. The measured resistance of the nanoparticle/metal interface in this structure is sufficiently small that it can be neglected when measuring the molecular resistance. For the molecular characterization studies discussed below, each sample was characterized using AFM, and when two or more nanoparticles were observed to bridge the gap in parallel, the current was normalized to the single-particle value assuming the parallel pathways were equivalent.

Current through Molecular Monolayers in Nanoparticle Bridges and Conducting Probe AFM Structures. Figure 3 shows current−voltage characteristics of two different molecule/nanoparticle bridge assemblies. Figure 3a shows the behavior

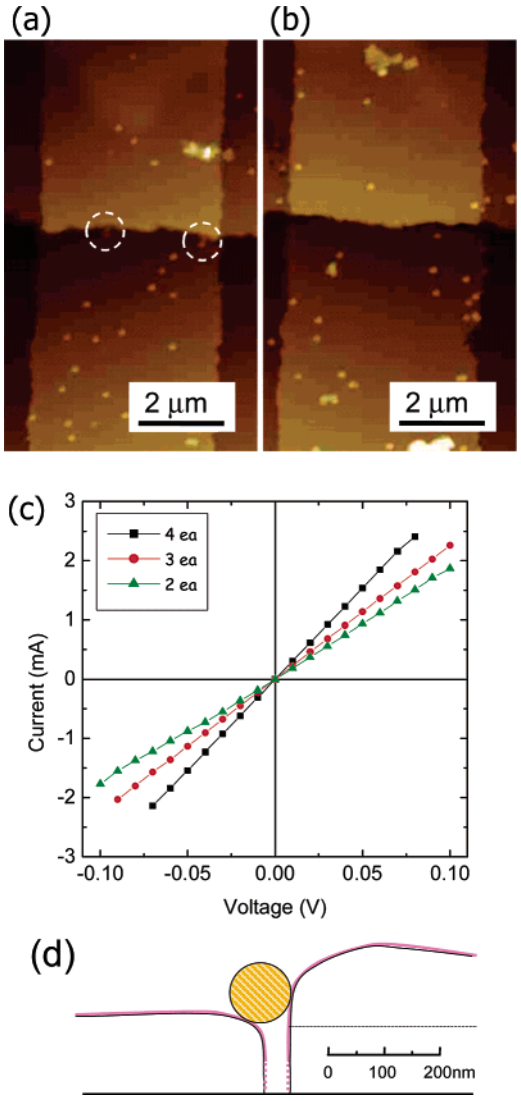

Figure 2. (a,b) Images of atomic force microscopy of nanoscale gaps after nanoparticle assembly, and (c) current−voltage behavior through the bridged nanoparticles without the addition of organic monolayers. (d) Sketch of the nanogap cross section with a nanoparticle in place, based on AFM image scans. Panel a shows two points connected by nanoparticles, whereas panel b shows no nanoparticles after nanoparticle solution treatment. The smallest current trace in panel a corresponds to the current for two particles, as measured with the sample shown in panel a. The sample in panel b shows current $<10^{-12}$ A.

when the gold electrode is coated with xylyldithiol, and Figure 3b shows that for hexanedithiol. The data in Figure 3a show an approximately ohmic $I-V$ relationship at room temperature for applied voltage of ±1 V, corresponding to a resistance of ~380 kΩ through one bridge, which is larger than the resistance through a nanoparticle bridge without the molecular monolayer. The $I-V$ curves in Figure 3b for the hexanedithiol show a nonlinear behavior and a significantly lower current level of $\sim 10^{-8}$ A at ±1 V. As expected, the alkanethiols showed larger resistances than those of alkanedithiols,[16,23,29] due to the higher resistance for the physical $-CH_3$/Au contact formed for the hexanethiol as compared to the S/Au bond for the hexanedithiol. The nonlinear $I-V$ trace in Figure 3b is typical of coherent nonresonant charge tunneling and has been widely observed for charge transport through molecular monolayers.[9,29,49] The resistance of hexanethiol in Figure 3b is $\sim 10^8$ Ω, which is

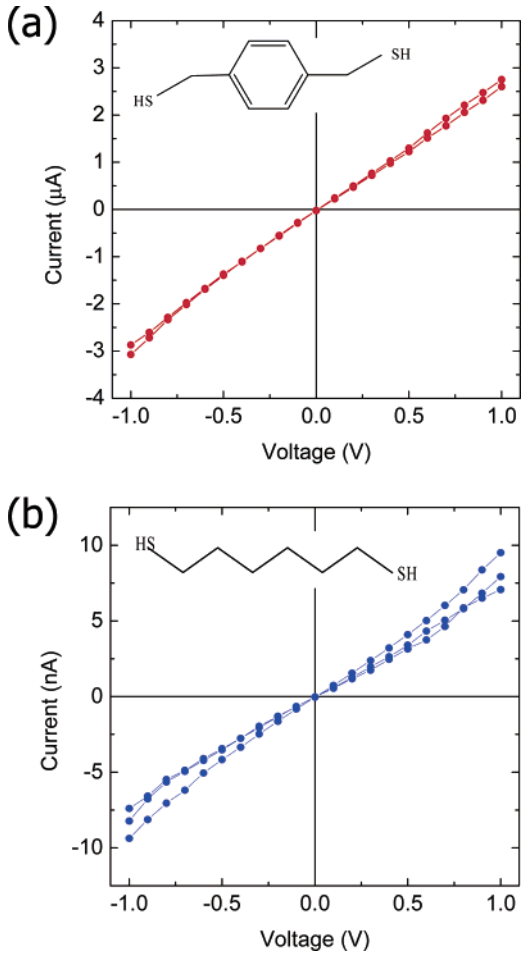

Figure 3. Current−voltage characteristics for two example molecule/nanoparticle/molecule assemblies. Molecular SAMs are (a) xylyldithiols and (b) hexanedithiols. Currents are measured under a vacuum and at room temperature.

somewhat higher than the value of $\sim 10^7$ Ω observed by Beebe et al. using conductive probe AFM,[12] consistent with a smaller contact area in the nanoparticle bridge structure as compared to the CPAFM measurement, as discussed below.

Figure 4 shows the $I-V$ behavior measured in the nanoparticle bridge structures for several alkanethiol molecules with different numbers of methylene units, $-(CH_2)_n-$, where $n = 6$ (C6SH), 10 (C10SH), and 12 (C12SH). For each type of molecule tested, up to ~10 measurements were done, and $I-V$ results are shown from two to four different measurements performed under the same conditions. The spread in the $I-V$ points represents typical variation in the current measurements. The lines represent typical fits to the average values. The same methodology was used to collect and plot $I-V$ data in Figures 5−7.

For further analysis of the monolayers, CPAFM analysis was also performed using a gold-coated AFM tip. A very small applied force was exerted (~2 nN) on the SAM in the contact AFM mode, and charge flow was measured using positive bias applied to the tip at room temperature. The measurements on each set of molecules were accomplished with the same tip to avoid possible errors from changing the tip. Figure 5 shows current−voltage curves for alkanethiol SAMs on Au measured with an Au-coated AFM tip. Increasing the length of alkanethiol

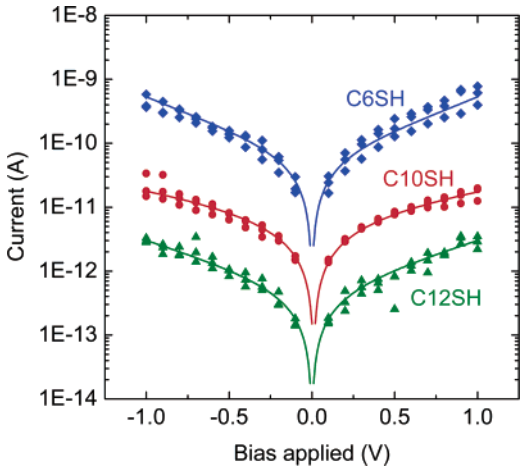

Figure 4. Current−voltage curves of alkanethiol SAMs measured in the metal/molecule/nanoparticle/molecule/metal bridge structure. The current values shown are the measured current multiplied by a factor of 2, to account for the two molecule sets in series in the bridge structure. The measured current is also divided by the number of nanoparticles assembled on the nanogap, as observed by AFM for each sample, to account for parallel conductance pathways through multiple nanoparticles. The data points are from several typical samples for each molecule type, and the solid line is a representative fit to the measured data to the Simmons conductance model.

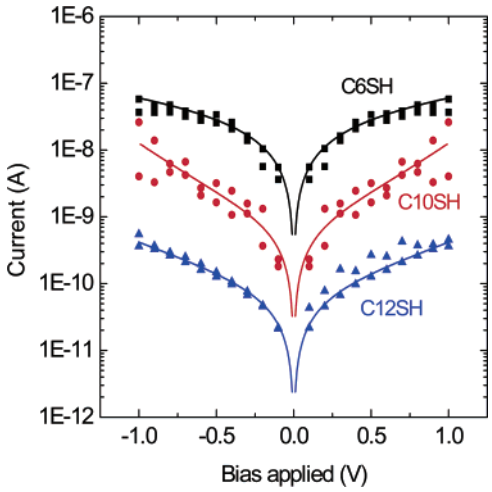

Figure 5. Current−voltage curves obtained from three different alkanethiol SAMs, measured using the conductive probe AFM structure with a gold tip. The data points are from several typical samples for each molecule type, and the solid line is a representative fit to the measured data to the Simmons conductance model.

leads to a decrease in the current, as observed in the nanoparticle bridge structure in Figure 4, although the absolute values of the current are quite different. The resistances of the alkanethiol monolayers measured by CPAFM are a factor of ~100−250 times smaller than those measured in the bridge structure for the C6, C10, and C12. The range of resistance ratios is likely related to variations in both the conducting probe and the nanogap structure. Generally, the smaller resistance is ascribed to a larger contact area for the CPAFM.

The $I-V$ behavior of alkylamine SAMs measured in the nanoparticle bridge structure is shown in Figure 6 as a function of number of methylene units, $-(CH_2)_n-$, where $n = 6$ (C6NH), 10 (C10NH), 12 (C12NH), and 18 (C18NH). Similar to the observation with the alkanethiols, the current levels decreased exponentially with chain length, as expected for a nonresonant electron-tunneling mechanism. We find that the current in

(49) Lee, T. H.; Wang, W. Y.; Reed, M. A. *Ann. N.Y. Acad. Sci.* **2003**, *1006*, 21−35.

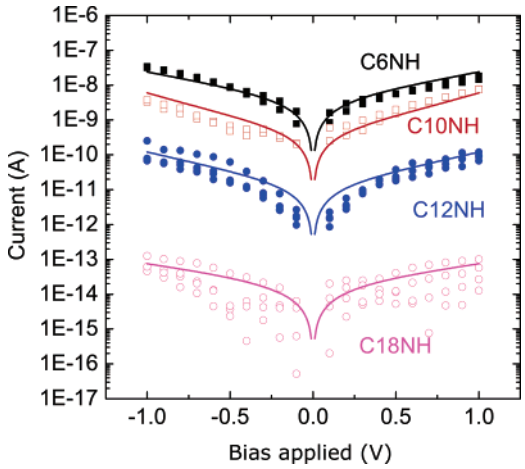

Figure 6. Current−voltage curves of alkylamine SAMs (C6NH, C10NH, C12NH, and C18NH) measured in the nanoparticle bridge structure and representative data fits. The current plots are constructed using the same method as in Figure 4 for the alkanethiol molecules.

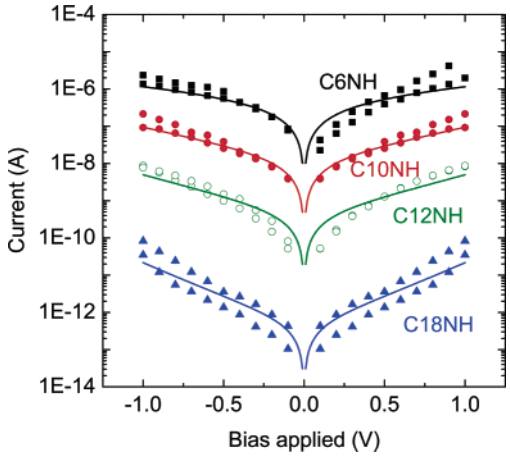

Figure 7. Current−voltage curves of alkylamine monolayers measured using the conductive probe AFM method and representative data fits. The current plots are constructed using the same method as in Figure 5 for the alkanethiol molecules.

multiple measurements tends to be more dispersed for the longest molecule studied ($n = 18$), as indicated by the spread in the data in Figure 6.

Figure 7 shows $I-V$ curves for alkylamine SAMs on Au measured with an Au-coated AFM tip. The current levels were higher than those for the same molecules measured in the nanoparticle bridge structure (Figure 6), consistent with the trend observed in the alkanethiol experiments. The current levels in Figure 7 were typically a factor of ~40 to 50 more than those in Figure 6 for the C6NH, C10NH, C12NH, and C18NH measured in the bridge structure. The magnitude of the difference between the nanoparticle bridge and CPAFM results for the alkylamine monolayers is smaller than in the alkanethiol case, possibly due to differences in contact areas for the different CPAFM measurements. The resistances of the alkylamine-terminated junctions are always measured to be less than those for the corresponding alkanethiol-terminated junctions. The data presented in Figures 3−7 show that the conductance measurements are sufficiently repeatable that general conclusions may be drawn regarding distinctions and trends within the molecular systems studied here.

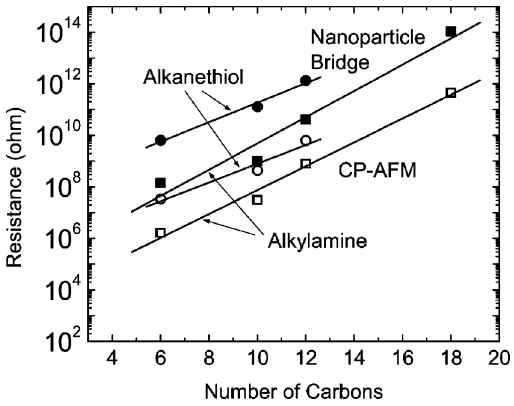

Figure 8. Semilog plot of average resistance values (measured at ±0.5 V bias) as a function of the number of methylene units in alkanethiol and alkylamine molecules measured in nanoparticle bridge structures (solid symbols) and by conducting probe AFM (open symbols). The circles correspond to measurements of alkanethiol monolayers, and the squares correspond to the alkylamine results.

Figure 8 shows the resistance calculated at ±0.5 V plotted versus number of carbons for each molecule in the nanoparticle bridge and CPAFM structures. The slope of the plot of ln(R) vs molecule length is used to evaluate the conductance decay factor, β, as discussed below.

4. Data Analysis and Discussion

Fitting of the $I-V$ Data and Current versus Molecule Length. For all the molecules studied, the current was observed to decrease exponentially with increasing number of methylene units in the molecule, as shown in Figure 8. This exponential dependence on molecule length is consistent with commonly observed coherent nonresonant charge tunneling, where the chemical potential of the metal electrode lies within the relatively large highest occupied molecular orbital−lowest occupied molecular orbital (HOMO−LUMO) gap of the molecule, and the tunneling barrier is higher than the applied bias ($V_{app} < \Phi_B/q$). In the low-bias regime, the Simmons model[38] is used to describe nonresonant tunneling:

$$I = \left(\frac{q}{4\pi^2\hbar s^2}\right)A\left\{\left(\Phi_B - \frac{qV}{2}\right)\exp\left[-\frac{2(2m)^{1/2}}{\hbar}\alpha\left(\Phi_B - \frac{qV}{2}\right)^{1/2}s\right] - \left(\Phi_B + \frac{qV}{2}\right)\exp\left[-\frac{2(2m)^{1/2}}{\hbar}\alpha\left(\Phi_B + \frac{qV}{2}\right)^{1/2}s\right]\right\} \quad (1)$$

where $\hbar = h/2\pi$ (h being Planck's constant), Φ_B is an effective barrier height in the insulator−metal interface, α is a dimensionless adjustable parameter, and m is the mass of an electron. The adjustable parameter α is used to correct the simple rectangular barrier model to account for the effective mass of the electron. The $I-V$ data in the low-bias regime (±1 V) in Figures 4−7 were fit to the Simmons model, and lines in each figure represent typical fits. The fits were obtained by choosing a pair of [Φ_B,α] values and varying both parameters sequentially to obtain a global minimum[50] by minimizing the value of $\Delta(\Phi_B,\alpha)$ over the range of ±1 V. The

(50) Wang, W. Y.; Lee, T.; Reed, M. A. *Rep. Prog. Phys.* **2005**, *68*, 523−544.

Table 1. Summary of Φ_B and α Parameters Obtained from Fitting of the *I*−*V* Data, and the Values for β Obtained from Plots of ln(*R*) at ±0.5 V versus Molecule Length[a]

	alkanethiol (–SH)			alkylamine (–NH)		
	α	Φ_B (eV)	β (Å^{-1})	α	Φ_B (eV)	β (Å^{-1})
nanoparticle bridge	0.90 ± 0.13	3.5 ± 1.2	0.79 ± 0.05	0.90 ± 0.13	2.0 ± 0.7	1.07 ± 0.05
CP-AFM	0.95 ± 0.09	3.4 ± 1.5	0.76 ± 0.05	1.0 ± 0.01	1.8 ± 0.7	0.97 ± 0.05

[a] The values shown for Φ_B and α were found to meet the global minimum of $\Delta(\Phi_B,\alpha)$.

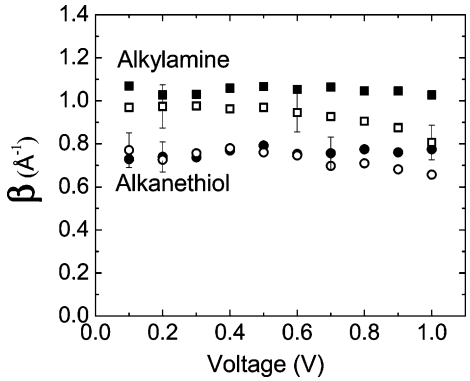

Figure 9. β (Å^{-1}) versus voltage for alkanethiols and alkylamines measured in bridge structures (filled symbols) and by conducting probe AFM (open symbols). β is approximately independent of bias for the range measured (up to 1 V), and β_0 is found to be 0.76 ± 0.03 for the alkanethiols and 0.99 ± 0.01 for the alkylamines.

value for $\Delta(\Phi_B,\alpha)$ is determined from the difference between the observed and calculated values of current ($I_{exp,V}$ and $I_{cal,V}$) summed over the voltage range considered:

$$\Delta(\Phi_B,\alpha) = (\sum | I_{exp,V} - I_{cal,V} |^2)^{1/2} \quad (2)$$

For each molecule and each test structure studied, a set of three to five *I*−*V* traces was fit, and the resulting optimum Φ_B and α for each data set, corresponding to molecules with amine or thiol termination in both the nanoparticle bridge and CPAFM configuration, were averaged to obtain the values shown in Table 1. The uncertainties in the table correspond to the range of values obtained for molecules of different lengths. For several data sets, a smaller voltage range was used in the fits, and in each case, the resulting best-fit optimum values for Φ_B and α were well within the uncertainty given in the table.

In the low-bias regime, eq 1 can be simplified to

$$R = R_0 \exp(\beta s) \quad (3)$$

where β is the tunneling decay factor and *s* is the length of the tunneling pathway along the alkane chains. A semilog plot of the average resistance values measured at 0.5 V bias as a function of the number of carbons in the molecule is shown in Figure 8, and the trends are consistent with eq 3. Using a value of 1.1 Å for the length of one methylene,[51] consistent with our ellipsometry results, the data in Figure 8 give β = 0.79/Å for the alkanethiol measured in the nanoparticle bridge structure. This and other β values obtained from the data in Figure 8 are shown in Table 1. The values of β were also obtained at other bias voltages, and the results of β vs bias for the four systems studied are shown in Figure 9. The error bars were typical values obtained from the quality of the fits. Generally, for both the alkanethiols and the alkylamines, the measured values of β varied little with changes in bias and did not depend on the nature of the measurement configuration (nanoparticle bridge or CPAFM). Some decrease in β with increasing voltage may occur for the alkylamines measured with CPAFM (open symbols in Figure 9), but the slope is small considering the distribution of the results. Tunneling decay coefficients are widely reported for alkanethiols on gold[6,9,10,16,29,51,52] and generally range from 0.7 to ~1.3/Å, with typically smaller values for molecules with covalent bonds at both ends as compared to only one end.[16] The values of β obtained for the alkanethiols in this work are near the lower end of this range. The value for the zero-field decay coefficient, β_0, obtained from a linear fit of β vs voltage in Figure 9, is found to be 0.76 ± 0.03/Å for the alkanethiols, which is less than the value of ~1.0/Å observed by Engelkes et al.[16] but is close to the value of ~0.8/Å observed by Wang et al.[52,53]

Current flow through alkylamine-terminated monolayers is not as widely studied as that in alkanethiols. The results in Figures 6−8 show that the measured currents through the alkylamine molecules are consistently 1 or 2 orders of magnitude higher than those in the alkanethiols with the same number of carbons, independent of whether the measurements are done by CPAFM or in the nanoparticle bridge structure. The increased conductance is generally expected to give rise to a reduced decay constant; however, the β values measured here for the alkylamines are somewhat larger than those for the alkanethiols. The β_0 value for alkylamine (~1.04 ± 0.03/Å in the nanoparticle bridge structure) is also larger than that obtained for the alkanethiols. Venkataraman et. al[54] reported β = 0.77/Å for alkanediamines measured at 25 mV, which is also smaller than the values reported here. While the reason for the observation of larger β values for the alkylamines is not presently clear, the differences observed between our work and that of Venkataraman et al.[54] could be due to differences in the details of the measurement approach, where our results are obtained in a vacuum without external applied force and their results were obtained under tension in the presence of a solvent. In addition, other recent results reported by Chen et al.,[55] also obtained in solvent, show smaller conductance values for amine-terminated alkanes as compared to similar thiol-terminated molecules.

The values for the estimated tunneling barrier heights and tunneling ideality factor obtained from the fits are also shown in Table 1. Care should be taken in analyzing the values obtained for the tunneling parameters from the Simmons fit. As pointed out by Engelkes et al.[16] and others,[6,10,56] the transport through molecular systems is not adequately modeled as a simple physical tunnel barrier. The mixing of the metal continuum states

(51) Smalley, J. F.; Feldberg, S. W.; Chidsey, C. E. D.; Linford, M. R.; Newton, M. D.; Liu, Y. P. *J. Phys. Chem.* **1995**, *99*, 13141−13149.
(52) Wang, W. Y.; Lee, T.; Reed, M. A. *Phys. Rev. B* **2003**, *68*, 035416.
(53) Wang, W. Y.; Lee, T.; Reed, M. A. *J. Phys. Chem. B* **2004**, *108*, 18398−18407.
(54) Venkataraman, L.; Klare, J. E.; Tam, I. W.; Nuckolls, C.; Hybertsen, M. S.; Steigerwald, M. L. *Nano Lett.* **2006**, *6*, 458−462.
(55) Chen, F.; Li, X.; Hihath, J.; Huang, Z.; Tao, N. *J. Am. Chem. Soc.* **2006**, 128, 15874−15881.
(56) Xue, Y.; Datta, S.; Ratner, M. A. *J. Chem. Phys.* **2001**, *115*, 4292−4299.

with the discrete molecule states at the metal/molecule junction generally gives rise to a density of states at the interface, and the value of Φ_B obtained from the fit to eq 1 is typically considered an effective transport barrier. The effective barrier is expected to be smaller than the barrier predicted from the estimated position of the HOMO or LUMO level of the molecular methylene chain relative to the metal Fermi level. The values for Φ_B and α obtained from fits to our data are larger than the values obtained by Wang et al. for tunneling through alkanethiols on gold,[52] although the standard deviation of our data sets leads to a relatively large uncertainty in the fits. The observed larger current flow through the alkylamine is consistent with the smaller barrier values extracted from the fits to the alkylamine data relative to the results from the alkanethiols.

When measured under conditions of charge tunneling at low bias in alkanethiol/Au junctions, the value R_0 obtained from the *y*-intercept of the lines in Figure 8 has previously been used by Frisbie et al.[9,12,16,27,28] as an effective contact resistance. This resistance can be related to the quantum conductance limit in the Landauer formalism (see below) but is used here simply as a parameter to compare transport through molecules with various end groups and various contact areas. For example, the value of R_0 obtained from the alkanethiols in the nanoparticle bridge structure in Figure 8 is 30.4 MΩ, which is larger than the value for the conducting probe AFM data ($R_0 = 184$ kΩ), consistent with a smaller contact area in the nanoparticle bridge structure. The value obtained for effective contact resistance for the alkanethiol in these CPAFM measurements is similar to the value of ∼50 kΩ measured by Frisbie et al. on the same molecular monolayer system,[16] but the resistance is expected to depend strongly on the load and tip geometry.[9,12,16,29] For the experimental results shown here for both the CPAFM and nanoparticle bridge geometry, the R_0 values obtained for the alkanethiols is consistently larger than that for the alkylamine molecules.

Scaling of Molecular Resistance and Estimated Contact Areas. From the data presented above for conduction through molecular monolayers, obtained using nanoparticle bridges and CPAFM, the current scaling can be examined for self-consistency and can be used to roughly estimate contact areas and the number of molecules being measured. This analysis can also qualitatively determine consistency and estimate approximate scaling factors between the two testing approaches used. The measurements of current through the xylyldithiol monolayers in the nanoparticle bridge structure in Figure 3 show a resistance of 4.0×10^5 Ω through the molecular ensemble. STM studies[57] report the resistance of a single xylyldithiol (*p*-xylene-dithiol or 4-methylbenzylmercaptan) molecule to be 18 ± 12 MΩ, which is close to the value of 22 MΩ reported for benzene-1,4-dithiol measured by mechanically controllable break junction.[24] Assuming simple linear scaling of molecular resistance in parallel,[17,31] and considering that the measured current represents charge flow through two resistors in series, the current values shown in Figure 3 are consistent with current flow through ∼100 xylyldithiol molecules on each side of the nanoparticle/metal bridge (i.e., ∼200 molecules in total). Considering that the projected area of a single molecule[57,58] is expected to be 0.214 nm^2, this suggests the contact area in the nanogap to be 20.1 nm^2 between the nanoparticle and the SAM. Similar scaling of the CPAFM data for the xylyldithiol results in a contact area of $\sim 3.2 \times 10^3$ nm^2, indicating that the CPAFM measurement used here results in a larger contact area than typically estimated by others.[9,59] The contact area of ∼20 nm^2 estimated for the nanoparticle bridge structure is consistent with the current measured through the gold nanoparticles without molecular monolayers present. The resistance of a gold nanoparticle alone (assuming negligible contact resistance) is equivalent to that of a gold wire (bulk resistivity $\sim 2.4 \times 10^{-8}$ Ω-m) with a cross-sectional area of 15−18 nm^2. This is <0.2% of the hemispherical area of the 80 nm nanoparticle, which is reasonably consistent with the expected physical contact area between the nanoparticle and the metal electrodes. Using a value of ∼100 molecules measured in each side of the molecule/nanoparticle/molecule junction, the current per molecule measured at 0.5 V for the C6, C10, and C12 alkanethiols is 200, 1.8, and 0.6 pA, respectively. These values are within the range of values estimated for single-molecule conduction by the Lindsay and Frisbie groups for the same molecules measured in CPAFM structures.[12,29,59]

Therefore, the observed trends in the *I*−*V* data are reasonably self-consistent between the testing approaches used and consistent with literature reports. The contact area for the 80 nm diameter nanoparticle bridge is roughly ∼10−20 nm^2, with on the order of 100 molecules measured in each contact (depending, of course, on the contact area per molecule and molecule density), and this contact area is a factor of ∼100 smaller than that obtained in our CPAFM measurement. We note that the symmetry of the *I*−*V* data in the CPAFM structure and the scaling of the data in the nanoparticle bridge structure are consistent with the assertion that the bridge structure is characterizing two equivalent resistors (i.e., two molecular ensembles) in series.

Transmission Probability. In the weak coupling limit, *I*−*V* data can be characterized in terms of the Landauer formalism,[60] where the net current is determined by the transmission probability as a function of energy, $T(E)$, and the quantum of conductance, $2q^2/h$. As shown by Engelkes et al.,[16] the overall transmission probability of the metal/molecule/metal junction can be written as the product $T_J = T_{C1}T_BT_{C2}$, where T_{C1} and T_{C2} are the transmissions through the contacts and T_B is the transmission through the bulk molecule. For the alkane, the transmission through the molecule can be expressed as a function of transmission through each methylene, T_{C-C}, so that $T_B = (T_{C-C})^n$, where *n* is the number of methylenes in the alkane chain. The net resistance can then be written in terms of the quantum of conductance, $2q^2/h$, and the number of parallel pathways for current flow, *N*, as

$$R_n = \frac{h}{2q^2N}\frac{1}{T_{C1}}\frac{1}{T_{C2}}\frac{1}{(T_{C-C})^n} \qquad (4)$$

In the limit of a single atom contact ($n = 0$) under ballistic transport conditions, the resistance would then be the quantum

(57) Andres, R. P.; Datta, S.; Dorogi, M.; Gomez, J.; Henderson, J. I.; Janes, D. B.; Kolagunta, V. R.; Kubiak, C. P.; Mahoney, W.; Osifchin, R. F.; Reifenberger, R.; Samanta, M. P.; Tian, W. *J. Vac. Sci. Technol. A* **1996**, *14*, 1178−1183.
(58) Strong, L.; Whitesides, G. M. *Langmuir* **1988**, *4*, 546−558.
(59) Salomon, A.; Cahen, D.; Lindsay, S.; Tomfohr, J.; Engelkes, V. B.; Frisbie, C. D. *Adv. Mater.* **2003**, *15*, 1881−1890.
(60) Nitzan, A. *Annu. Rev. Phys. Chem.* **2001**, *52*, 681−750.

conductance limit: $h/2q^2 = 12.9\ k\Omega$. Considering the measured resistance values and the current scaling discussed above, the measured current values are consistent with T_{C1} and $T_{C2} \ll 1$. Moreover, comparing the resistance of the hexanedithiol shown in Figure 3 to the results for hexanethiol in Figure 4, the ratio of the transmission coefficient for the gold/methyl ($T_{C2} = T_{CH}$) and that for the gold/thiol contact ($T_{C2} = T_{SH}$) is estimated to be $T_{CH}/T_{SH} = 3.8 \times 10^{-2}$, which is close to the value of $\sim 5 \times 10^{-2}$ reported by Englekes et al.[16] Relating eq 4 to eq 3 for resistance versus chain length, the data for alkanethiol and alkylamine versus chain length (Figure 8) give a estimates for T_{C-C} of $\sim 0.33 \pm 0.05$ for the alkanethiol and $\sim 0.46 \pm 0.05$ for the alkylamine, where the errors reflect the standard deviation of the linear fit. These values are reasonably similar to the value reported by Englekes (~ 0.33) for alkanethiols and alkanedithiols contacting a set of various metals.[16,59] We note that, in the Landauer formalism, the transmission values at the molecule/metal interface cannot be evaluated independently from the molecule because electron-state coupling at the metal/molecule interface must necessarily include a contribution from the molecular orbital states in the bridge molecule itself.[60] Even so, if it is assumed that the methyl/nanoparticle resistances and the contribution of the alkane chains to the interface resistance are approximately the same in the alkanethiol/gold and alkylamine/gold junctions, the resistance values measured in the nanoparticle bridge structure can be used to obtain a transmission coefficient ratio $T_{SH}/T_{NH} \approx 1 \times 10^{-2}$. The results obtained with the CPAFM give a somewhat larger ratio, $T_{SH}/T_{NH} \approx 9 \times 10^{-2}$, but both results show larger current through the amine than through the thiol end groups.

Mechanisms Affecting Resistance in Alkylamine/Gold Junctions. As discussed above, even when tunneling models can give a reasonable fit to charge transport data through molecular systems under low bias, transport at the interface must consider the nature and extent of the mixing between molecular orbitals and the metal density of states at the metal/molecule interface. However, modeling the results in terms of tunnel barriers can give insight into differences at different metal/molecule contacts. The barrier heights estimated from the global-minumum fitting of the Simmons model are shown in Table 1. Barrier values of 3.5 ± 1.2 and 3.4 ± 1.5 eV are obtained for alkanethiols in the nanoparticle bridge and CPAFM structures, respectively. Wang et al.[50] reported a somewhat smaller barrier value, $\Phi_B = 1.42-1.83$ eV, for alkanethiols sandwiched between two Au electrodes in a 45 nm silicon nitride pore. Relatively high barrier heights are expected due to the lack of electronic coupling at the CH_3/Au interface. Values for the correction factor α obtained from the optimized fits of the data in Figures 4−6 are also shown in Table 1. The value for α is found to range from 0.9 to 1.0 for the different head groups and is also relatively independent of the measurement structure used. Reported values of α typically range from 0.59 to 0.68 for current flow though alkanethiols,[49,53] which is smaller than the values reported here. The values for α in the CPAFM measurement may be somewhat larger than those in the nanogap, with no clear trend relative to the different head groups.

The higher current observed for the amine/gold junction relative to the thiol/gold junction is likely related to a very different charge transport mechanism in the amine-terminated monolayers relative to the thiol-terminated junctions. While other mechanisms, such as thermionic emission, cannot be ruled out without more detailed temperature-dependent analysis, the data scaling is consistent with tunneling, which is widely observed[53,55] in saturated chain molecules. For charge flow dominated by tunneling, the higher current in the amine/gold junction could be related to differences in the net interfacial dipole, which will depend on the linker/Au bond structure, as well as the linker/molecule dipole, which both depend on the linker chemistry. The amine/Au bond is expected to be more ionic, with more charge transfer than for the thiol/Au bond. The different charge transfer will affect the magnitude of the interface dipole and the effective barrier height at the contact. However, charge transport in molecular junctions is expected to be physically linked to the extent of state mixing at the metal/molecule interface, so that the energy and spatial extent of mixed electron states within the molecule and near the contact must also be considered. Different state mixing at the thiol/Au and amine/Au interfaces is consistent with calculations by Venkataraman et al.[54] that show that the amine/gold bonding proceeds through hybridization of the nitrogen lone pair with the gold, leading to a hybrid state that is directed along the bond axis, whereas the thiol/Au bonding results in states more localized near the bonding contact. Other preliminary results of density functional calculations[61] are consistent with this difference in bonding structure and indicate a somewhat higher current at small bias through the amine/Au bond relative to the thiol/Au bond. Moreover, reactions with any available oxygen will depend on the nature of molecule end group and will likely affect the bonding and wave function mixing at the molecule/electrode contact. Recently, Chen et al. showed a somewhat smaller conductance and smaller β for alkanediamines compared to alkanedithiols for single molecules measured in a STM break-junction geometry.[55] This disparity between the results of Chen et al. and those shown here could relate to different metal contact atom arrangement or molecular conformation (i.e., azimuthal angle or bending) that depends on molecular density and/or test-bed geometry. For example, a higher tunneling probability could be expected if the flexible alkanes are under more compression in the contact methods used here, as compared to tension in the single-molecule STM approach.

5. Summary and Conclusions

Room-temperature current versus voltage measurements through self-assembled monolayers in molecule/nanoparticle/molecule bridge structures and in conducting probe AFM show reasonable agreement in terms of current scaling and magnitude of current flow through several molecule systems. The scaling of the $I-V$ data at low bias through xylyldithiol, hexanedithiol, alkanethiols (C6SH, C10SH, and C12SH), and alkylamines (C6NH, C10NH, C12NH, and C18SH) is reasonably modeled by nonresonant tunneling. The tunneling decay parameters obtained from the alkanethiol monolayers are observed to be nearly independent of applied bias, and the values are reasonably close to those previously reported for the same molecule/metal system. A smaller resistance is routinely observed when the thiol/Au contact is replaced with an amine/Au contact in the alkyl chains. The difference is ascribed to differences in charge transfer and wave function mixing at the metal/molecule contact, including effects of nitrogen lone pair interaction with the gold

(61) Kim, G.; Wang, S.; Lu, W.; Buongiorno-Nardelli, M.; Bernholc, J., private communication, 2006.

which result in a hybrid wave function directed along the molecule bond axis. In addition, molecular conformation and oxidation in the contact region will also depend on end group and should be considered to understand conduction in molecular junctions. These results demonstrate that, in addition to bond strength, bond configuration at the metal/molecule contact is important for optimized charge-transfer characteristics in applications involving electronically active molecules.

6. Experimental Details

The solvents used included ethanol (anhydrous with water content $\leq$0.5%) from Fisher Scientific and tetrahydrofuran (anhydrous, 99.9% inhibitor-free) from Sigma-Aldrich and were used as received. The concentration of the respective self-assembled monolayer in the deposition experiments was 1 mM. Alkanethiols purchased from Sigma-Aldrich included C6SH (95%), C10SH (96%), and C12SH (98.5%). The alkylamines purchased from Sigma-Aldrich included C6NH (99%), C10NH (95%), and C12NH (98%); C18NH (99%) was purchased from Fluka.

The thicknesses of monolayer films were measured using an Auto EL ellipsometer (Rudolph Technologies, Flanders, NJ) at an angle of incidence $\Phi = 70°$ and a wavelength $\lambda = 632.8$ nm. Atomic force microscopy (AFM) imaging was performed in the tapping mode under ambient conditions using an AFM from Digital Instruments (Santa Barbara, CA) with a Nanoscope IIIa controller. SuperSharpSilicon probe tips (frequency, 260−410 kHz, spring constant, 21−78 N/m; SSS-NCH, Nanoscience Instruments, Phoenix, AZ) were used with a typical tip radius of curvature of 2 nm, providing high-resolution AFM images in the nanogap region.

For the conducting probe AFM measurements, current was measured through the monolayers using AFM tips (DNP-S20, spring constant, 0.06−0.58 N/m; Veeco Probes, Santa Barbara, CA) coated with Ti (5 nm) and Au (45 nm), deposited by electron-beam evaporation. The current was measured in ambient conditions with the AFM tip in a stationary position, electrically wired to a Keithley 230 voltage source and a Keithley 6512 electrometer (Keithley Instruments, Cleveland, OH). For the nanoparticle bridge configuration, the $I-V$ measurements were carried out in a probe station (model ST-100, Janis Research, Wilmington, MA) under vacuum of $\sim 5 \times 10^{-4}$ Torr using a Keithley 230 voltage source and a Keithley 6512 electrometer. Electrical characterization instruments are computer-controlled using an electronic interface and LabView software from National Instruments (Austin, TX).

Acknowledgment. The authors acknowledge support from the National Science Foundation awards DMR 0303746 and CTS 0626256. We thank G. Kim, M. Buongiorno-Nardelli, and J. Bernholc for sharing results before publication, as well as Nongjian Tao and Chris Gorman for helpful discussions.

JA064968S